Wave-equation migration velocity analysis for VTI media using optimized implicit finite difference

Yunyue (Elita) Li

ABSTRACT

Anisotropic wave-equation migration velocity analysis (WEMVA) requires fast and accurate wave modeling at all angles. I use an optimized implicit finite difference one-way propagation engine to improve both the efficiency and accuracy of this process. In this implicit finite difference scheme, anisotropic parameters η and δ are mapped into two finite difference coefficients, α and β. When computing the perturbed wavefields from model perturbation, I apply a chain rule to link the wave equation with the actual anisotropic parameters via the finite difference coefficients. I test the implementation by impulse responses in both 2D and 3D. The sensitivity kernels for wave-equation reflection tomography confirm the theoretical understanding that waves have a higher sensitivity for η at large angles and a higher sensitivity for vertical velocity at small angles.

INTRODUCTION

Building an anisotropic model requires accurate wave field descriptions at all angles, both in simple and complex geological settings. Therefore, instead of using travel times and ray paths, we use the wave fields as the carrier of the model information (Li and Biondi, 2011a; Li et al., 2012; Li, 2012). Many choices for wavefield propagators may be considered. On one hand, the one-way wave propagators (Li, 2012) excel in speed but lose their accuracy rapidly with the increasing propagation angle. On the other hand, the two-way wave propagators (Li et al., 2012) are more accurate in modeling waves at large angles but their computational costs are less affordable.

Therefore, I use an optimized implicit finite difference propagator first developed by Shan (2006). In this optimized implicit finite difference scheme, the anisotropic parameters η and δ contribute to the wave-equation implicitly via two finite difference parameters α and β. Tables of α and β with respect to sets of discrete η and δ values are precomputed before propagation by minimizing the difference between the true dispersion relationship and its rational series approximation at different wavenumbers. This table-driven, implicit finite difference method handles lateral variations and is accurate up to 60° in a vertical transverse isotropic (VTI) medium.

When perturbing the wave-equation around its current state, the finite difference coefficients α and β are perturbed. These perturbations are then translated into the

anisotropic parameters η and δ using the chain rule. Tables of numerical derivatives of the finite difference coefficients α and β with respect to the anisotropic parameter η are also precomputed from the previous coefficients tables.

Finally, I test this implicit finite difference implementation by 2D and 3D impulse responses for vertical velocity v_v and η. The results verify the theoretical understanding of the WEMVA operator for anisotropic models.

OPTIMIZED IMPLICIT FINITE DIFFERENCE FOR VTI MEDIA

Assuming the S-wave velocity is much slower than the P-wave velocity, we can approximate the dispersion relationship for VTI media as follows (Shan, 2009):

$$S_z = \sqrt{\frac{1-(1+2\delta)S_r^2}{1-2\eta(2\delta+1)S_r^2}}, \tag{1}$$

where $S_z = \frac{k_z}{w/v_v}$, $S_r = \frac{k_r}{w/v_v}$ and $k_r = \sqrt{k_x^2+k_y^2}$. Anisotropic parameter δ relates the vertical P-wave velocity v_v with the NMO velocity v_n, while the anellipticity parameter η relates the horizontal velocity v_h with the NMO velocity v_n. Shan (2009) suggests that the exact dispersion relationship 1 can be approximated by a rational function $R_{n,m}(S_r)$:

$$R_{n,m}(S_r) = \frac{P_n(S_r)}{Q_m(S_r)}, \tag{2}$$

where

$$P_n(S_r) = \sum_{i=0}^{n} a_i S_r^i \tag{3}$$

and

$$Q_m(S_r) = \sum_{i=0}^{m} b_i S_r^i. \tag{4}$$

Moreover, when the polynomials in equations 3 and 4 are of the same degree, namely $m = n$, dispersion relationship 2 can be further split as follows:

$$S_z = 1 - \sum_{i=1}^{n} \frac{\alpha_i S_r^2}{1-\beta_i S_r^2}. \tag{5}$$

The coefficients α_i and β_i can be obtained by solving the least-square problem below:

$$\min \sum_{S_r} \left(\sqrt{\frac{1-(1+2\delta)S_r^2}{1-2\eta(2\delta+1)S_r^2}} - \left(1 - \sum_{i=1}^{n} \frac{\alpha_i S_r^2}{1-\beta_i S_r^2}\right)\right)^2. \tag{6}$$

For second-order coefficients the exact and approximated dispersion curves are shown in Figure 1(a), given $\eta = 0.14$ and $\delta = 0.2$. Curve A is the exact dispersion relation

from Equation 1. Curve B is obtained from a previous estimation by Ristow and Ruhl (1997), and curve C is obtained using the optimized coefficients. Apparently, the dispersion relation using the optimized coefficients is a better approximation compared with the previous method which uses Taylor expansion and assumes weak anisotropy. The relative errors between these two approximated curves and the exact dispersion curve are plotted in Figure 1(b). Within a tolerance of 1% relative error in the dispersion relation, the optimized dispersion is accurate up to 60°, while the Taylor approximation is only accurate up to 30°.

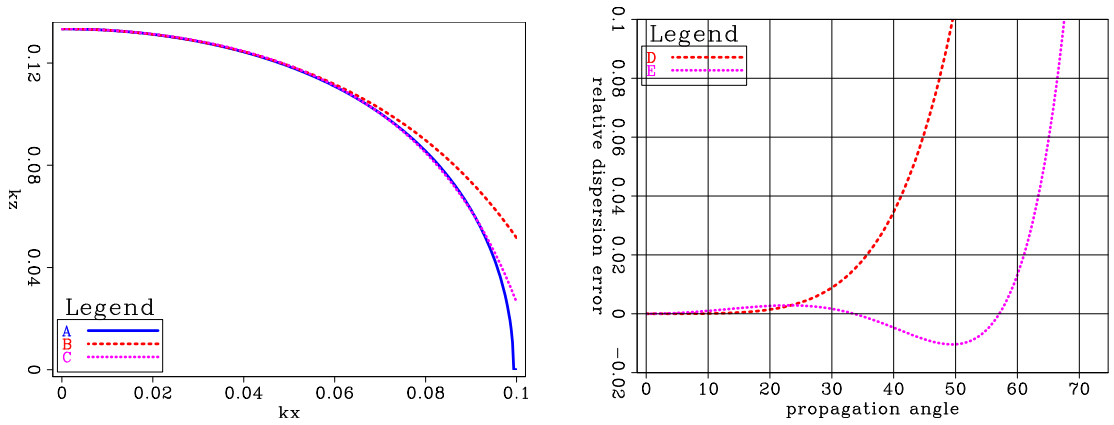

(a) (b)

Figure 1: (a) Dispersion relation curves: A, exact dispersion relation curve from equation 1; B, approximated dispersion curve from weak anisotropy and Taylor expansion; C, approximated dispersion curve from optimization. (b) Relative dispersion error: D, relative error between B and A; E, relative error between C and A. [**ER**]

The tables for coefficients α and β for η ranging from 0 to 0.15 and δ ranging from -0.004 to 0.2 are shown in Figure 2. In general, parameter α is more sensitive to the change in δ than to the change in η. Parameter β has similar sensitivities to both η and δ.

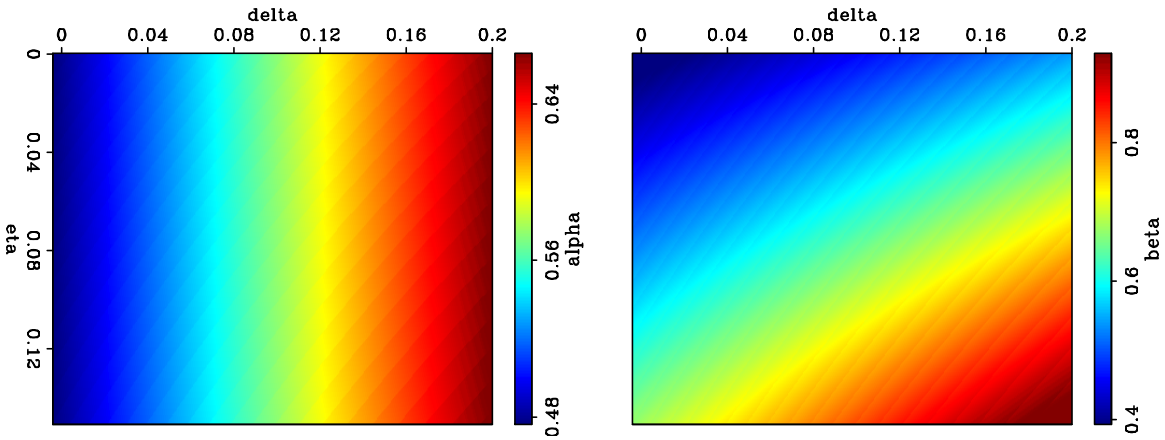

Figure 2: (a) Table for α and (b) table for β at discrete η and δ locations. [**ER**]

IMPULSE RESPONSE OF THE IMAGE-SPACE WAVE-EQUATION TOMOGRAPHY OPERATOR

The core of anisotropic image-space wave-equation migration velocity analysis is the tomography operator $\mathbf{T}$, which relates the perturbation in the anisotropic models ($\Delta\mathbf{m}$) to to the perturbation in the image (ΔI) and vice versa. Namely,

$$\Delta I = \mathbf{T}\Delta\mathbf{m}, \tag{7}$$
$$\Delta\mathbf{m} = \mathbf{T}'\Delta I, \tag{8}$$

where $\mathbf{m} = [v_v\ \eta]$.

I refer the readers to Li and Biondi (2010) for a detailed derivation for the tomographic operator.

A different approximation to the exact dispersion relation leads to a different perturbed wave fields due to a perturbation in the model parameters. When the only available data come from surface seismic surveys, parameter δ is the least constrained (Plessix and Rynja, 2010; Li and Biondi, 2011b). Therefore, I assume the δ model is perfectly obtained from other sources of data and keep it fixed throughout the inversion. I will invert for v_v and η in this study.

In the downward extrapolation, the wavefield at the next depth (P_{z+1}) can be computed from the wavefield at the current depth (P_z) according to the following equation:

$$P_{z+1} = P_z e^{ik_z dz}, \tag{9}$$

where $i = \sqrt{-1}$, dz is the extrapolation distance in depth and k_z can be obtained from the first-order approximation of the dispersion relation 5:

$$k_z = \frac{w}{v_v}\left(1 - \frac{\alpha\frac{k_r^2}{(w/v_v)^2}}{1-\beta\frac{k_r^2}{(w/v_v)^2}}\right). \tag{10}$$

Dispersion relation 10 can be further simplified to polynomials using Taylor expansion:

$$\begin{aligned} k_z &= \frac{w}{v_v}\left(1 - \alpha\frac{k_r^2}{(w/v_v)^2}\left(1+\beta\frac{k_r^2}{(w/v_v)^2}\right)\right) \\ &= \frac{w}{v_v}\left(1 - \alpha\frac{k_r^2}{(w/v_v)^2} - \alpha\beta\frac{k_r^4}{(w/v_v)^4}\right). \end{aligned} \tag{11}$$

Therefore, the perturbed wavefield is

$$\Delta P_{z+1} = e^{ik_z dz} i dz P_z \Delta k_z, \tag{12}$$

with

$$\Delta k_z = \frac{\partial k_z}{\partial v_v}\Delta v_v + \frac{\partial k_z}{\partial \eta}\Delta\eta, \tag{13}$$

$$\frac{\partial k_z}{\partial v_v} = -\frac{w}{v_v^2}\left(1 + \alpha\frac{k_r^2}{(w/v_v)^2} + 3\alpha\beta\frac{k_r^4}{(w/v_v)^4}\right), \tag{14}$$

and

$$\frac{\partial k_z}{\partial \eta} = -\frac{w}{v_v}\left(\frac{\partial \alpha}{\partial \eta}\frac{k_r^2}{(w/v_v)^2} + \left(\frac{\partial \alpha}{\partial \eta}\beta + \alpha\frac{\partial \beta}{\partial \eta}\right)\frac{k_r^4}{(w/v_v)^4}\right). \tag{15}$$

Since the finite difference parameters α and β are obtained by optimization, the derivatives in Equation 15 are obtained numerically by taking derivatives along the η axis in Figure 2. The tables of the derivatives of the coefficients with respect to η are shown in Figure 3.

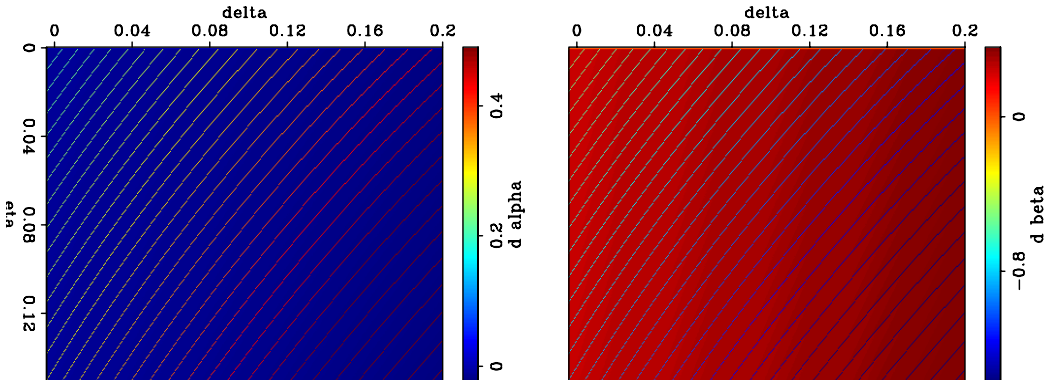

Figure 3: (a) Table for $\frac{\partial \alpha}{\partial \eta}$ and (b) table for $\frac{\partial \beta}{\partial \eta}$ at background η and δ locations. [**ER**]

I test the implementation of the adjoint tomographic operator using this optimized implicit finite difference scheme in a homogeneous background VTI medium with $v_v = 2000$ km, $\eta = 0.09$ and $\delta = 0.05$. The synthetic data is produced by Born modeling with a horizontal reflector at the depth of 1500 km. The input of the adjoint tomographic operator is a spike in the image space $\Delta I = \delta(x, y, z = 1500)$. The dominant frequency of the source wavelet is 20 Hz, and the samplings in all directions are 10 m.

I first test the adjoint operator in 2D. A source and receiver pair is collocated at $x = y = z = 0$. The top row in Figure 4 shows the back-projected vertical velocity v_v gradient and η gradient when source-receiver offset is zero. These back projections are often referred as banana-donut kernels in the literature when transmission waves are under study (eg. Marquering et al. (1998, 1999); Rickett (2000)). Similar reflection tomography sensitivity kernel analysis for isotropic WEMVA operator can be found in Sava (2004) and Xie and Yang (2009).

Compared with the η gradient, the v_v gradient has a nearly uniform strength with depth, while the η gradient fades away as the wavepath moves away from the source and the receiver location. Also, the dominant energy of the η gradient points to the opposite direction of the v_v gradient points. In fact, the η gradient is not reliable and should be ignored because the wave that travels in the vertical direction is not sensitive to η.

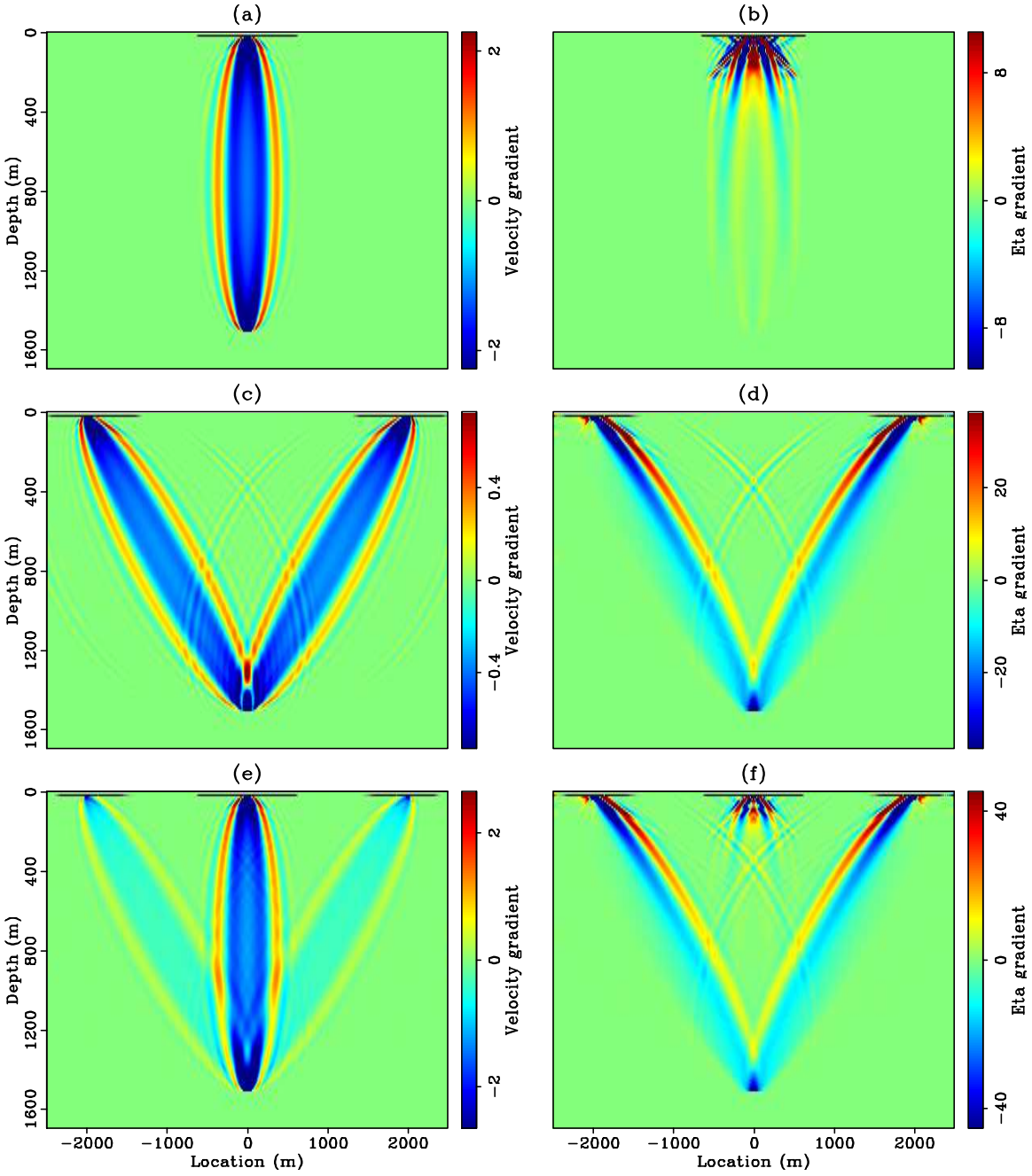

Figure 4: 2D impulse responses for vertical velocity (left column) and η (right column). Top row: zero offset impulse responses; middle row: impulse responses when source-receiver offset is 4 km; bottom row: summation of the two rows above. [**ER**]

When the source-receiver offset is 4 km, the gradients are shown in the middle row in Figure 4. Clearly, the back projections are spread along the wavepaths from the source to the perturbed image point and from the perturbed image point to the receiver. In this case, the gradients in both v_v and η point in the same direction. Comparing the gradients in the cases of zero and nonzero offset, one can see that the vertical waves are more sensitive to v_v, and the waves traveling at a large angle (36° to the vertical in this case) are more sensitive to η. The bottom row in Figure 4 shows the summation of the gradients in these two cases, and confirms these observations.

The 3D extension of this method is straightforward. The sensitivity kernels for v_v and η in 3D are shown in Figures 5 and 6. A source and receiver pair with 4 km offset are located at $y = 0$. The 3D sensitivity kernels carry the same characteristics as the 2D kernels, only expanding to the crossline direction.

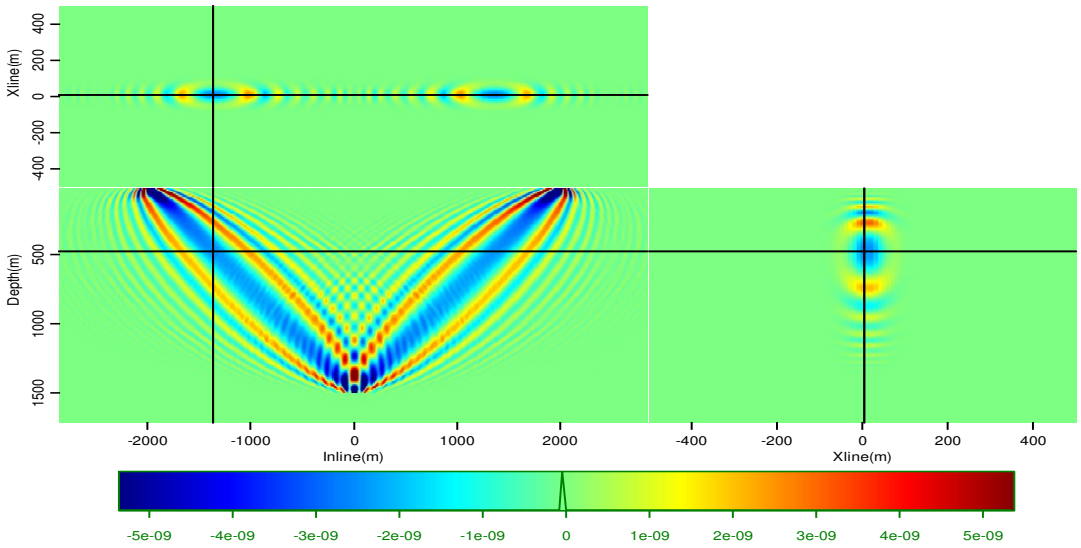

Figure 5: 3D v_v kernel. [**CR**]

CONCLUSIONS AND DISCUSSIONS

In this paper, I use an optimized implicit finite difference one-way propagation engine to improve both the efficiency and accuracy for anisotropic WEMVA. By precomputing the tables for the finite difference coefficients, the cost of this VTI extrapolation is similar to an isotropic implicit finite difference scheme. With the optimized coefficients, the dispersion relation is accurate up to 60°. To compute the disturbed wave fields due to the perturbation in the models, the numerical derivatives of the optimized coefficients with respect to η are also precomputed.

I test the VTI implicit finite difference scheme by impulse responses in both 2D

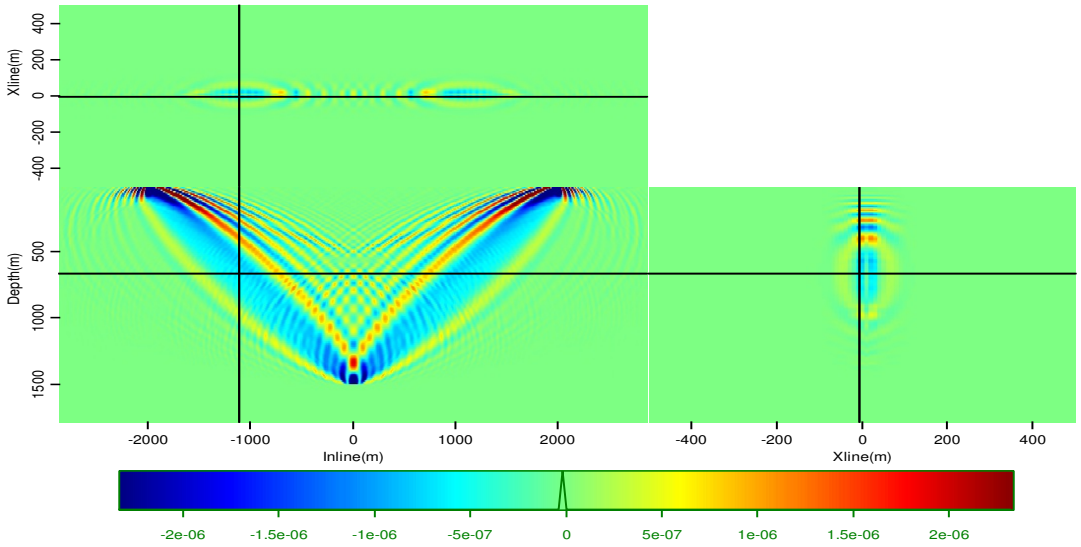

Figure 6: 3D η kernel. [**CR**]

and 3D. These impulse responses of the adjoint anisotropic WEMVA operator from a spike perturbation in the image space have a familiar banana-donut sensitivity kernel shape for both v_v and η. The amplitudes in these impulse responses show different sensitivities for different parameters with different source-receiver geometries. The waves traveling vertically have higher sensitivity to v_v and the waves traveling at large angles have higher sensitivity to η. Therefore, the 3D sensitivity kernels can also be used for acquisition design before exploration when specific parameters are under consideration.

REFERENCES

Li, Y. and B. Biondi, 2010, Wave-equation tomography for anisotropic parameters: SEP-Report, **140**, 49–60.

———, 2011a, Migration velocity analysis for anisotropic models: SEG Expanded Abstract, **30**, 201–206.

Li, Y. E., 2012, Wave-equation migration velocity analysis for anisotropic models on 2-D ExxonMobil field data: SEP-Report, **147**, 83–94.

Li, Y. E. and B. Biondi, 2011b, Migration velocity analysis for anisotropic models: SEP-Report, **143**, 21–32.

Li, Y. E., P. Shen, and C. Perkins, 2012, VTI migration velocity analysis using RTM: SEP-Report, **147**, 57–72.

Marquering, H., F. A. Dahlen, and G. Nolet, 1998, Three-dimensional waveform sensitivity kernels: Geophysical Journal International, **132**, 521–534.

———, 1999, Three-dimensional sensitivity kernels for finite-frequency traveltimes: the banana-doughnut paradox: Geophysical Journal International, **137**, 805–815.

Plessix, R.-E. and H. Rynja, 2010, VTI full waveform inversion: A parameterization study with a narrow azimuth streamer data example: SEG Expanded Abstracts, **29**, 962–966.

Rickett, J., 2000, Traveltime sensitivity kernels: Banana-doughnuts or just plain bananas?: SEP-Report, **103**, 63–71.

Ristow, D. and T. Ruhl, 1997, Migration in transversely isotropic media using implicit operators: SEG Expanded Abstract, **67**, 1699–1702.

Sava, P., 2004, Migration and velocity analysis by wavefield extrapolation: PhD thesis, Stanford University.

Shan, G., 2006, Optimized implicit finite-difference migration for VTI media: SEP-Report, **124**, 279–292.

———, 2009, Optimized implicit finite-difference and Fourier finite-difference migration for VTI media: Geophysics, WCA189–WCA197.

Xie, X.-B. and H. Yang, 2009, The finite-frequency sensitivity kernel for migration residual moveout and its applications in migration velocity analysis: WTOPI Report, **16**.